Results in Chemistry 21 (2026) 103078

Contents lists available at ScienceDirect

Results in Chemistry

journal homepage: www.sciencedirect.com/journal/results-in-chemistry

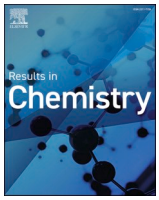

Synthesis and biological evaluation of heteroarylnitrile derivatives for motile ciliogenesis☆

Gwi Bin Lee [a,1], Gopalakrishnan Chandrasekaran [b,1], Da Bin Jeon [b,1], Chan-Young Park [b], Parvathi Varier Sundareswaran [b], Byeong Wook Choi [a], Pyeongkeun Kim [a], Jihyeon Yoon [a], Seok-Yong Choi [b,**], Jin Hee Ahn [a,c,*]

[a] Department of Chemistry, Gwangju Institute of Science and Technology, Gwangju 61005, Republic of Korea
[b] Department of Biomedical Sciences, Chonnam National University Medical School, Gwangju, Republic of Korea
[c] JD Bioscience, 208 Cheomdan-gwagiro, Buk-gu, Gwangju 61005, Republic of Korea

ARTICLE INFO

Keywords:
Motile cilia
FOXJ1
Multiciliated cells(MCCs)
Ciliogenesis
Small-molecule therapeutics

ABSTRACT

Motile cilia play a critical role in maintaining tissue homeostasis by driving fluid movement and clearing inhaled particles or pathogens. Dysfunction of these organelles underlies a range of ciliopathies, most notably affecting the respiratory system. Building on previous studies that identified molecules promoting motile cilia formation, we tried to discover novel small molecules that enhance motile ciliogenesis. To this end, we conducted a phenotype-based high-throughput screen using a Tg(foxj1a:eGFP) zebrafish reporter line, which led to the identification of a new chemotype hit. Subsequent structure–activity relationship (SAR) studies resulted in the development of compound **19b**, which promoted motile cilia formation in zebrafish embryos. Its efficacy was further validated in ex vivo air–liquid interface (ALI) cultures of mouse tracheal epithelial cells, where treatment with **19b** significantly increased the number of multiciliated cells. These findings suggest that compound **19b** is a useful chemical probe for studying ciliogenesis and a potential lead for therapeutic development in motile ciliopathies.

1. Introduction

Motile cilia exist as microscopic cellular extensions projecting from the cell surface. Coordinated ciliary motion produces directional fluid flow, which is essential for both developmental processes and the maintenance of homeostasis [1–3]. In contrast to primary cilia, which function primarily as sensory receptors, rhythmic beating of motile cilia arises from an axonemal architecture composed of paired microtubules arranged in a 9 + 2 pattern, together with dynein-driven motors and radial spoke elements. The critical roles of motile cilia include the clearance of mucus from the respiratory tract, the transport of eggs within the oviduct, sperm motility, the breaking of left-right asymmetry at the embryonic node, and the circulation of cerebrospinal fluid in the brain ventricles [2,4]. Motile ciliopathies commonly stem from genetic defects affecting proteins that either form the ciliary apparatus or regulate pathways regulate pathways required for ciliogenesis and ciliary signaling [4–6]. In our previous study, we found that motile ciliogenesis in zebrafish and mice is supported by Wnt-dependent Ca^{2+} signaling involving the PLC–IP3 pathway and Connexins [7].

The development and maintenance of motile cilia are tightly regulated processes. FOXJ1, a forkhead box transcription factor, serves as a central transcriptional regulator governing motile cilia development. It functions as a key regulator, activating the genes required for the formation and operation of cilia [1,8–10]. FOXJ1 orchestrates the differentiation of specialized ciliated cells, driving their transformation into efficient ciliary machines. In mouse models, loss of FOXJ1 resulted in the failure of motile axoneme formation in multiciliated cells, while increased FOXJ1 expression was sufficient to drive motile cilia formation across multiple tissues [10–12]. Targeting the FOXJ1 pathway offers a promising new therapeutic strategy for restoring ciliary function

☆ This article is part of a Special issue entitled: 'Medicinal Chemistry' published in Results in Chemistry.

* Corresponding author at: Department of Chemistry, Gwangju Institute of Science and Technology, Gwangju 61005, Republic of Korea.
** Corresponding author.
E-mail addresses: Zebrafish@chonnam.ac.kr (S.-Y. Choi), jhahn@gist.ac.kr (J.H. Ahn).
[1] These authors equally contributed to this work.

https://doi.org/10.1016/j.rechem.2026.103078
Received 10 September 2025; Received in revised form 17 January 2026; Accepted 19 January 2026
Available online 20 January 2026

and alleviating motile ciliopathies. Based on these findings, high-throughput screening and molecular biology are facilitating the discovery of compounds that can modulate FOXJ1, potentially correcting the molecular defects associated with these disorders.

Although known therapeutic agents associated with ciliopathies temporarily relieve symptoms, they do not achieve enhanced motile cilia [11]. In our previous study, we identified a new molecule that enhances motile cilia production. This new small molecule, which significantly enhances FOXJ1 promoter activity, demonstrated efficacy in the *Tg(foxj1a:eGFP)*^{hsc16} zebrafish model, which expresses a fluorescent reporter gene (eGFP) regulated by the *foxj1a* promoter, thereby selectively identifying cell populations harboring motile cilia [12,13].

Using a system established by our team, we aimed to expand our compound library and identify novel chemotypes with potentially distinct efficacy and ADMET profiles. Through a high-throughput(HTS) evaluation of a diverse chemical library from the Korea Chemical Bank (KCB) [7,11,13], we discovered a Hit **1** that stands out as a new chemotype for further validation. This resulting compound not only broadens the chemical space around our previous leads but also provides a potential scaffold for enhancing foxj1 expression. Here, we present the development and characterization of new heteroarylnitrile derivatives targeting motile cilia.

2. Results & discussion

2.1. Phenotype-Based screening in a zebrafish model

Tg(foxj1a:eGFP)^{hsc16}, a zebrafish model driven by the *foxj1a* promoter expressing EGFP was used to identify new compounds that enhance ciliogenesis. Compound **1** was identified as a hit from the Korea Chemical Bank library (Fig. 1).

To optimize the hit, we performed structural modifications of three parts (A, B, and C) (Fig. 2). Compound **1** (the hit) possesses a unique structure featuring fused hetero-bicyclic and nitrile moieties, representing a novel scaffold compared to previously reported molecules. The imidazopyrimidine core can be derivatized with various fused heterocycles, and the nitrile group is amenable to modification by several bioisosteres, including carboxylic acids and esters. First, efforts were focused on the part A ring with diverse heterobicycles.

The hit **1** and several heteroarynitrile derivatives **6a-b** and **9a-d** were synthesized according to Scheme 1. The commercially available 2-bromopyridine **2** was converted into substituted pyridines **3** by the nucleophilic substitution with lithioacetonitrile, followed by Knoevenagel condensation with imidazo[1,2-*a*]pyrimidine-3-carbaldehyde **4** in the presence of piperidine to give hit compound **1.** Heterocyclic compound **7a** was converted to aromatic aldehyde **8a** by Vilsmeier–Haack formylation. *N*-ethyl formyl indole **8d** was prepared by N-alkylation with

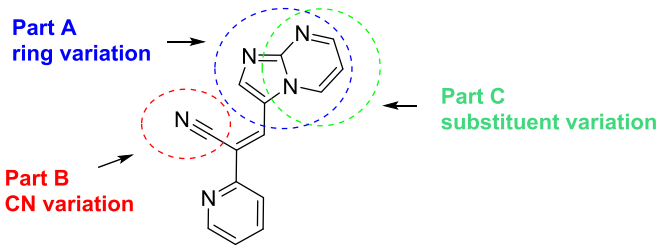

Fig. 2. Optimization strategy of compound 1.

bromoethane. Then, Knoevenagel condensation of 2-(pyridin-2-yl) acetonitrile **5a-b** and **8a-d** with pyridine intermediate **3** using piperidine provided compounds **6a-b** and **9a-d.**

Compounds **14** and **16** were prepared as shown in Scheme 2. Commercially available picoline **10** reacted with diethyl carbonate **11** under LDA condition, followed by hydrolysis of ester to afford acetic acid **13**. Compound **13** was condensed with 1H-indole-3-carbaldehyde under decarboxylative Knoevenagel condition to give **14**. Notably, ^{1}H NMR analysis consistently demonstrated a 16–18 Hz coupling between the vinylic protons, indicative of the exclusive presence of trans isomers in the synthesized compound **14**. Meanwhile, compound **12** was reacted with aldehyde **8c** using $TiCl_4$-pyr to obtain compound **15**, followed by hydrolysis to afford carboxylic acid **16** (Scheme 2).

Compounds **19a-j** were prepared as shown in Scheme 3. Indole derivatives (**17a-j**) were formylated under Vilsmeier-Haack conditions to give **18a-j**, followed by coupling with **3** to give the corresponding **19a-j**.

Hit **1** showed enhanced *foxj1a* expression at 5 μM compared to the control (DMSO). Building on the structure of Hit **1**, a series of diverse derivatives (**6a-b** and **9a-d)** were synthesized and subsequently evaluated for their efficacy in enhancing motile ciliogenesis (Table 1). Initially, Hit **1** was optimized by modifying the imidazopyrimidine ring with various heterocycle derivatives. We introduced 6,6-bicyclic moieties (**6a-b**) and it was found that the 6, 6-membered ring showed weaker activity than the 6, 5-membered ring (**9a-d**). Therefore, diverse 6, 5-membered rings were synthesized and evaluated. Compounds containing indazole **9b** and NH-indole **9c** showed enhanced activity. Notably, compound **9c** demonstrated superior activity compared to **9b**, while compound **9d** without NH proton displays decreased activity.

Next, part B optimization was conducted out and the results were summarized in Table 2. Compound **14** exhibited decreased activity in the absence of the nitrile group. Similarly, compounds substituted with ester or carboxylic acid groups were found to exhibit reduced biological activity relative to the active compound **9c** (Table 2**).**

We further optimized **9c** with diverse substituted indole and the results are summarized in Table 3. Compound **19b** containing a methoxy

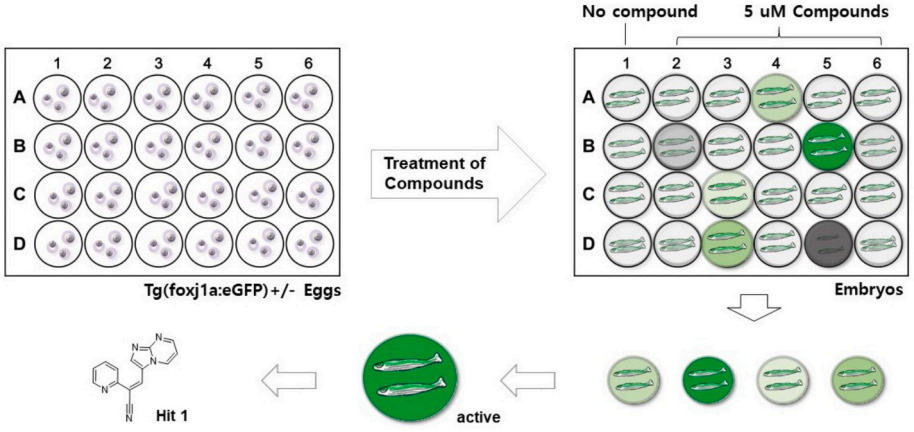

Fig. 1. Phenotypic High-Throughput Screening: An Overview.

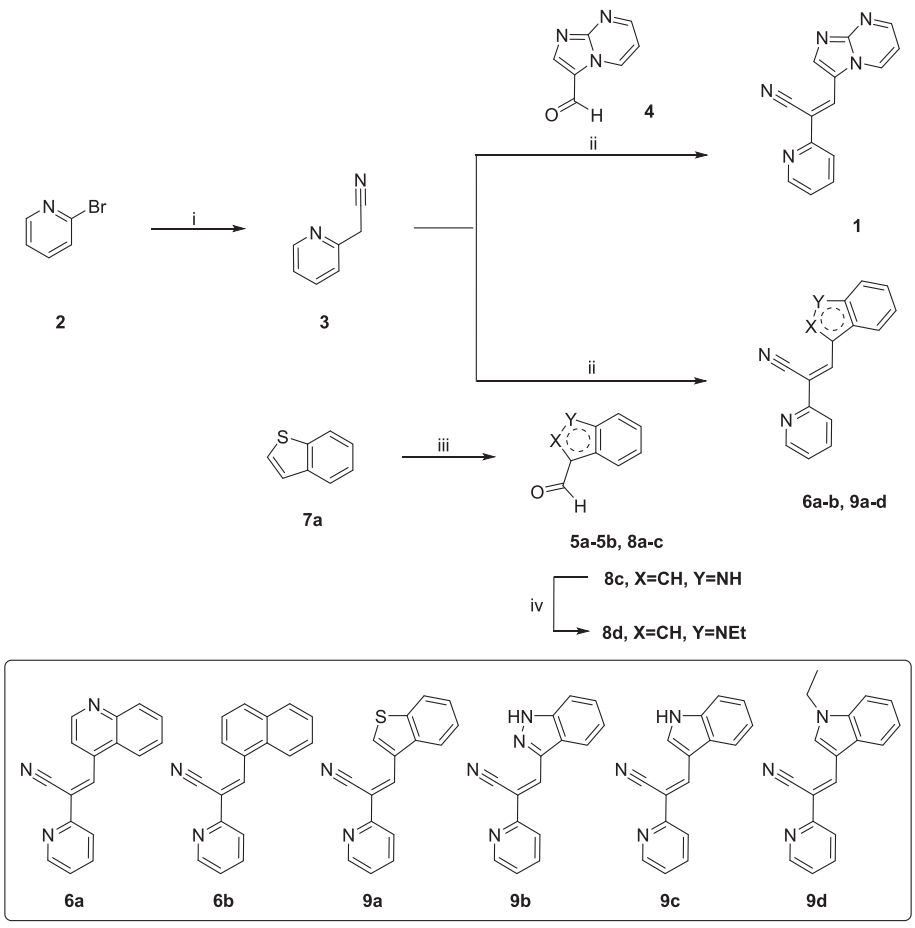

Scheme 1. Synthesis of pyridine derivatives containing fused heteroaromatic bicycles. Reagents and conditions: i) n-BuLi, ACN, THF, −78 °C to rt., ii) cat. Piperidine EtOH, reflux, 16 h. iii) $POCl_3$, DMF, reflux, 24 h, iv) EtBr, NaH, THF, rt., 24 h.

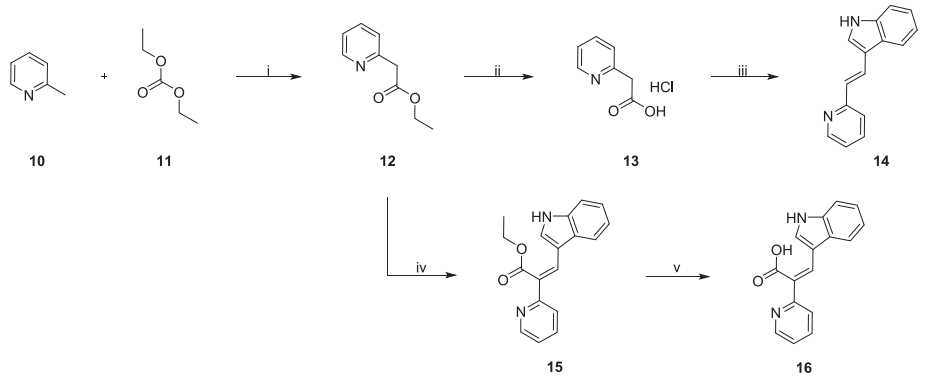

Scheme 2. Synthesis of compound **14–16**. Reagents and conditions: i) LDA, THF, −78 °C, 1 h and then rt., 30 min. ii) LiOH·H_2O, EtOH, H_2O, 50 °C, 2 h. iii) 1H-indole-3-carbaldehyde, TEA, dioxane and then piperidine, 90 °C, overnight. iv) $TiCl_4$, Pyr, dry THF, 0 °C, rt. and then reflux, 24 h. v) LiOH·H_2O, EtOH, H_2O, 50 °C, 2 h.

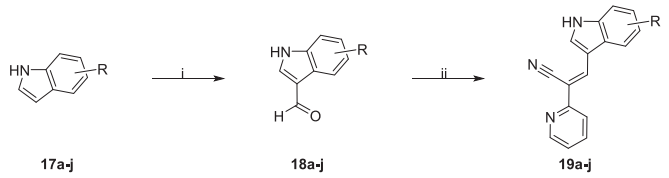

Scheme 3. Synthesis of compound **19a-j**. Reagents and conditions: i) $POCl_3$, DMF, reflux, 24 h, ii) **3**, cat. Piperidine EtOH, reflux, 16 h.

group at the 5-position of the indole ring, showed increased activity. However, other methoxy derivatives (**19a**, **19c**, and **19d**) were inactive. Consequently, further modifications were conducted by introducing additional substituents at 5-position. Substitutions with 5-methyl group **19e** significantly decreased the activity. The 5-methoxy group of **19b** was subsequently replaced with fluoro (**19f**), bromo (**19g**), nitro (**19h**), and nitrile (**19i**) group. Compound **19f** showed no activity or highly toxic, while compounds **19g** and **19h** exhibited reduced activity, with a particularly marked decrease observed for **19i**. Overall, a reduction in activity was observed for these three compounds. The ester (**19j**) group

Table 1
SAR data of pyridine derivatives containing fused bicycles.

Compound	R	Foxj1 Activity at 5 μM (% increase in GFP intensity over DMSO treatment)
1	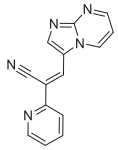	40
6a	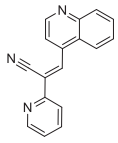	10
6b	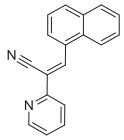	20
9a	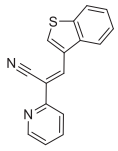	25
9b	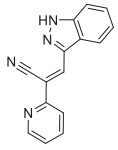	70
9c	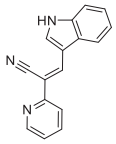	80
9d	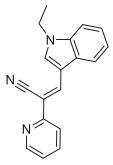	43

The potency of the compounds on the expression of FOXJ1 compared to DMSO treatment was examined.

at 5-position demonstrated moderate efficacy. From the results, **19b** was selected for further evaluation.

Motile cilia are observed in the spinal cord (SC) ependymal cells and pronephric duct (PN) of zebrafish larvae [10]. We examined the dose-dependent effect of **19b** on motile ciliary cells using the *Tg(foxj1a: eGFP)* zebrafish line, in which motile ciliary cells in the zebrafish SC and PN are labeled with EGFP driven by the *foxj1a* promoter [10]. *Tg(foxj1a: eGFP)* embryos treated with varying concentrations of **19b** showed that EGFP expression significantly increased in both the SC and PN, at the minimum effective concentrations of 1 μM and 2.5 μM, respectively (Fig. 3a-c). This indicates that **19b** enhances Foxj1a expression in these

Table 2
SAR of pyridine derivatives via replacement of nitrile group.

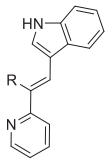

Compound	R	Foxj1 Activity at 5 μM
9c	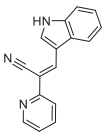	80
14	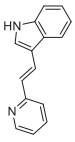	62
15	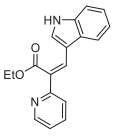	64
16	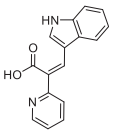	69

The potency of the compounds on the expression of FOXJ1 compared to DMSO treatment was examined.

tissues.

We further evaluated **19b** in mouse tracheal epithelial cells (mTECs) cultured ex vivo. mTECs treated with 5 μM **19b** from air-liquid interface (ALI) day 0 for 4 days displayed a significant increase in the number of MCCs and mRNA compared to DMSO-treated controls (Fig. 4a, b, c). This suggests that **19b** activates motile ciliogenesis in mammalian airway epithelium, mirroring its effect on *foxj1a* promoter activity in zebrafish motile ciliary cells.

Motile ciliogenesis is orchestrated by a hierarchical transcriptional cascade involving **GMNC, MCIDAS** and **FOXJ1/RFX** transcription factors [14]. This core regulatory network integrates multiple upstream signaling pathways, including **Wnt/β-catenin**, **Notch**, and **planar cell polarity** pathways, which have been shown to influence ciliary differentiation and organization [15–17]. As such, we propose that **compound 19b** may exert its effects by modulating one or more of these transcriptional regulators and/or signaling pathways.

3. Conclusion

Motile cilia are important microtubule-containing structures that coordinated ciliary motion produces a directional fluid flow, which is crucial for both developmental processes and the maintenance of homeostasis. Dysregulation of ciliogenesis and ciliary length has profound implications for ciliopathy pathogenesis. Effective pharmacological treatments for ciliopathies remain needed, underscoring the critical need for new therapeutic development. Here, we demonstrate that a synthetic small molecule capable of activating foxj1a promoter activity promotes the regeneration of motile cilia. Our analysis indicates that both ciliation and ciliary length regulation are promising therapeutic targets for disorders characterized by absent or dysfunctional cilia. Notably, compound **19b** emerges as a leading candidate, providing a

Table 3
SAR of pyridine derivatives via introduction of substituents in indole.

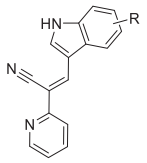

Compound	R	Foxj1 Activity at 5 μM
9c	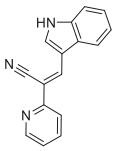	80
19a	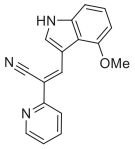	10
19b	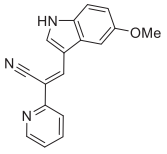	99
19c	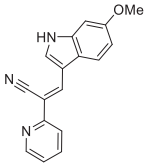	10
19d	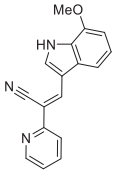	9
19e	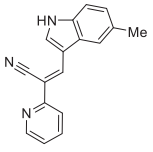	53
19f	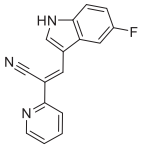	N.D. (dead)
19 g	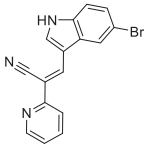	55

Table 3 (*continued*)

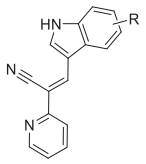

Compound	R	Foxj1 Activity at 5 μM
19 h	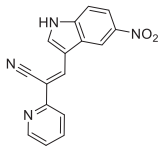	51
19i	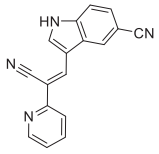	28
19j	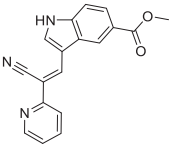	61

The potency of the compounds on the expression of FOXJ1 compared to DMSO treatment was examined. ND, not determined.

foundation for the future development of pharmacological strategies to treat ciliopathies. Compound **19b** demonstrates potent induction of the foxj1a promoter activity at 10 μM resulting in a significant enhancement of the promotion of foxj1a promoter activity in zebrafish. Furthermore, **19b** shows a dose-dependent response with regard to the promotion of foxj1a promoter activity and effectively increases the number of MCCs in ex vivo assay. Compound **19b** represents a promising probe for potential therapeutic applications in motile ciliopathies.

4. Materials and methods

4.1. General methods for chemistry

All solvents and chemicals were purchased from commercial suppliers and used without further purification. Analytical thin layer chromatography (TLC) was performed on precoated silica gel 60 GF254 plates. Visualization on TLC was achieved by use of UV light (254 nm). All the reported yields are isolated yields after column chromatography or crystallization. ^{1}H NMR spectra and ^{13}C spectra were recorded on a JEOL JNM-ECS400 spectrometers at 400 MHz for ^{1}H NMR and 100 MHz for ^{13}C NMR respectively. The chemical shift (δ) is expressed in ppm relative to tetramethylsilane (TMS) as an internal standard, and $CDCl_3$-d, DMSO-d_6 were used as solvents. Data are reported as follows: chemical shift, multiplicity of peaks expressed as s (singlet), d (doublet), t (triplet), q (quartet), dd (doublet of doublets), td (triplet of doublets), qd (quartet of doublets), dt (doublet of triplets), m (multiplet), coupling constants (Hz) and integration. HRMS data were obtained by a JMS 700 (JEOL, Japan). High-performance liquid chromatography (HPLC) analyses were performed with an Agilent HPLC system equipped with a PDA detector and an Agilent SB-C18 column (1.8 μm, 2.1 x 50 mm). The mobile phase consisted of buffer A (ultrapure H_2O containing 0.1% trifluoroacetic acid) and buffer B (chromatographic grade CH_3CN) for method. Flow rate was 0.5 mL/min. Liquid chromatography coupled to time-of-flight mass spectrometry (LC-QTOF-MS) data were collected using a Bruker UHPLC system for chromatographic separation, coupled

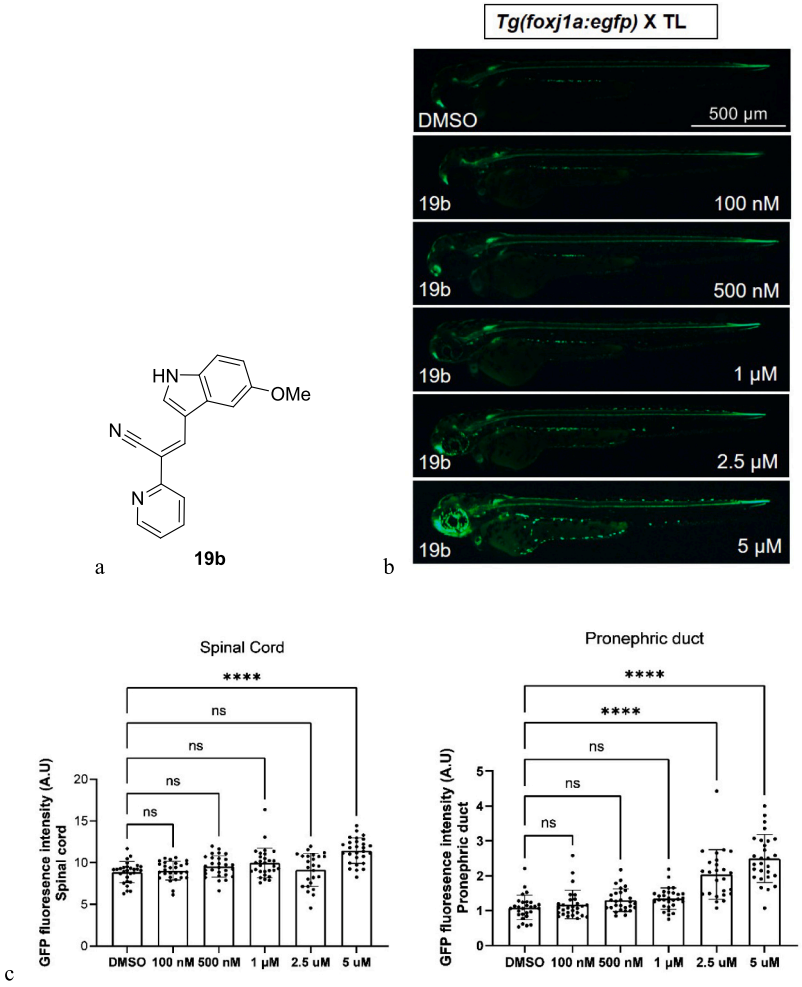

Fig. 3. 19b enhances Foxj1a expression in the spinal cord and pronephric duct. (a) structure of **19b** (b) *Tg(foxj1a:eGFP)* embryos at 1 day post-fertilization were treated with the indicated concentration of **19b** for 24 h and imaged with fluorescence stereomicroscopy. Scale bar = 500 μm. **(c)** Quantification of EGFP intensity from images in (b). $n = 28$ embryos except for the 2.5 μM group ($n = 25$ embryos). Data are presented as mean ± SD. **** $P < 0.0001$ by one-way ANOVA with Tukey's HSD post hoc test. ns, not significant.

to an Intensity solo2 C18 column (2.0 μm, 2.0 x 100 mm), maintained at 40 °C.

4.2. Synthesis of (Z)-3-(5-methoxy-1H-indol-3-yl)-2-(pyridin-2-yl) acrylonitrile (19b)

Step 1. To a solution of dry acetonitrile (0.4 mL, 7.86 mmol) in dry THF (4 mL) and n-BuLi (3 mL, 7.60 mmol, 2.5 M solution in hexane) were added at −78 °C and under N_2 [18]. A solution of commercially available 2-bromopyridine **2** (300 mg, 1.90 mmol) in dry THF (9 mL) was added dropwise. The mixture was stirred at −78 °C for 2 h and was then warmed to r.t. and stirred for 2 h. After the reaction mixture was diluted with water and extracted with ethyl acetate. Organic layer was separated, dried over anhydrous sodium sulfate, filtered and the solvent evaporated under reduced pressure. The residue was purified by column chromatography to give 2-(pyridin-2-yl)acetonitrile **3** (180 mg, 80%) as a yellow oil. ^{1}H NMR (400 MHz, Chloroform-*d*) δ 8.57 (ddd, $J = 5.0, 1.9, 1.0$ Hz, 1H), 7.73 (td, $J = 7.7, 1.8$ Hz, 1H), 7.42 (ddq, $J = 7.8, 1.0, 0.6$ Hz, 1H), 7.30–7.22 (m, 1H), 3.93 (s, 2H).

Step 2. A mixture of 2-(pyridin-2-yl)acetonitrile (**3**) (50 mg, 0.42 mmol), 5-methoxy-1*H*-indole-3-carbaldehyde (**18b**) (74 mg, 0.42 mmol) and piperidine (four drops) in EtOH was refluxed for 16 h. After the reaction mixture was cooled to room temperature (RT), the residue was diluted with diethyl ether and the resulting solid was filtered, washed with diethyl ether, and dried under vacuum. The residue was purified by silica gel column chromatography to give *(Z)*-3-(imidazo [1,2-*a*]pyrimidin-3-yl)-2-(pyridin-2-yl)acrylonitrile 1 (15 mg, 13%) as a light yellow solid, m.p.:193–196 °C. ^{1}H NMR (400 MHz, DMSO-d_6) δ 12.06 (s, 1H, NH), 8.66 (s, 1H, CH), 8.65–8.59 (m, 1H, C-H_{pyr}), 8.43 (d, $J = 2.7$ Hz, 1H, C-H_{indole}), 7.92–7.80 (m, 2H, C-H_{pyr}), 7.51 (t, $J = 1.7$ Hz, 1H, C-H_{indole}), 7.43 (d, $J = 8.8$ Hz, 1H, C-H_{pyr}), 7.32 (ddd, $J = 6.5, 4.9, 1.5$ Hz, 1H, C-H_{pyr}), 6.88 (dt, $J = 8.8, 1.7$ Hz, 1H, C-H_{indole}), 3.85 (d, $J = 1.2$ Hz, 3H, OMe); ^{13}C NMR (100 MHz, DMSO-d_6) δ 155.06, 152.41, 149.42, 137.41, 136.88, 130.79, 128.84, 128.06, 122.29, 119.84, 119.33, 113.31, 113.22, 110.53, 101.93, 100.34, 55.52. HRMS(FAB) *m/z* calculated for $C_{23}H_{26}N_5O_3$ [M + H]+ 276.1137, found 276.1138; HPLC purity 97.08%.

4.3. Reagents and chemicals

All ACS-grade reagents and chemicals were purchased from Sigma-Aldrich (St. Louis, MO, USA).

4.4. Ethics

All animal experiments were conducted with the approval of the Institutional Animal Care and Use Committee (IACUC) at Chonnam National University Medical School (Project No. H-2024-13). Animal procedures complied with the relevant guidelines and regulations set forth by the Republic of Korea.

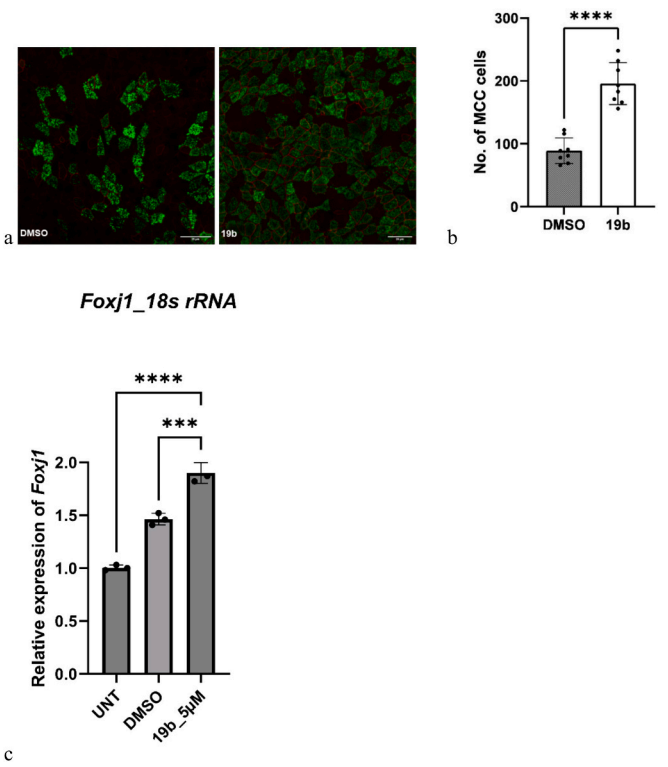

Fig. 4. 19b increases the number of respiratory multiciliated cells (MCCs). (**a**) Mouse tracheal epithelial cells (mTECs) were treated with 5 μM **19b** from air-liquid interface (ALI) day 0 for 4 days, and were immunostained with anti-acetylated α-tubulin (green; a motile cilia marker) and anti-ZO-1 (purple; a tight junction marker) antibodies. DMSO was used as a vehicle control. Scale bar = 25 μm (DMSO); 20 μm (**19b**). **(b)** The number of MCCs was quantified in each of eight independent images. Data are presented as mean ± SD. **** $P <$ 0.0001 using unpaired student's *t*-test. (**c**) mTECs were left alone or treated with DMSO or 5 μM **19b** and processed for mRNA extraction. Subsequently, qPCR with *Foxj1* primers was carried out and its expression was normalized to *18S rRNA* (*Rn18s*). The experiment was repeated thrice (technical replicates). Data are presented as mean ± SD. *** $P <$ 0.001 and **** P < 0.0001 by one-way ANOVA with Tukey's HSD post hoc test. (For interpretation of the references to colour in this figure legend, the reader is referred to the web version of this article.)

4.5. Zebrafish husbandry

The wild-type (WT) zebrafish (TL) were sourced from the Korea Zebrafish Resource Center (KZRC), Hwasun, Korea. Transgenic *Tg (foxj1a:egfp)*^{hsc16} line was generously provided by Dr. Brian Ciruna (Ontario, Canada) [12,13]. All zebrafish were housed in the aquatic facility at Chonnam National University Medical School (Hwasun, Korea), where they were kept at 28 °C under a regulated 14-h light and 10-h dark cycle, following institutional maintenance protocols. For compound screening, we selected EGFP-positive embryos generated by outcrossing the *Tg(foxj1a:egfp)*^{hsc16} line with TL zebrafish.

4.6. Mouse husbandry

Male C57BL/6 mice (6–8 weeks old; Samtaco BIO KOREA) were maintained in a controlled environment (21 ± 2 °C, 55 ± 10% humidity) with a 12-h light/dark cycle. A commercial diet and water were provided ad libitum. Following the final experimental procedure, mice were euthanized using CO_2 inhalation for subsequent tissue collection.

4.7. HTS of the chemical library for enhanced foxj1a promoter activity

Tg(foxj1a:eGFP)^{hsc16} zebrafish were outcrossed to TL zebrafish and their resulting embryos with uniform EGFP expression and synchronized developmental stages were selected for screening. Subsequently, these selected embryos at one day post-fertilization (dpf) were manually dechorionated and transferred into sterile 96-well plates (SPL Life Sciences, 30096), with three embryos per well containing 198 μL of E3 medium (5 mM NaCl, 0.17 mM KCl, 0.33 mM $CaCl_2$, and 0.33 mM $MgSO_4$). Chemicals from the Korea Chemical Bank were first dissolved in DMSO to prepare 5 mM stock solutions, which were then diluted to 500 μM as working solutions. For compound treatment, 2 μL of the 500 μM working solution was dispensed into each well, yielding a final concentration of 5 μM. Control wells contained 1% DMSO (*v*/v) as the vehicle control. Embryos were exposed to the compounds for 24 h. At two dpf, embryos were examined under a fluorescence stereomicroscope (Leica MZ16 FA) to assess EGFP signal along the SC. Following anesthesia with 1.5 mg/mL tricaine (ethyl 3-aminobenzoate methanesulfonate salt; Sigma-Aldrich, E10521), embryos were mounted in 3% methylcellulose to restrict movement during imaging. Embryos displaying morphological abnormalities and/or developmental delay were excluded from further analysis. Compounds that increased EGFP expression in the SC by more than twofold compared to DMSO were indentified as hits. **19b** was further assessed for increase in EGFP expression in the SC and PN with varying concentrations.

4.8. ALI culture of mouse tracheal epithelial cells (mTECs)

Primary TECs were isolated from adult WT C57BL/6 mice aged 6–8 weeks and cultured using an mTECs differentiation protocol described previously [13]. Tracheae were digested overnight (O/N) at 4 °C with pronase (Roche, 10165921001) to release epithelial cells. To selectively remove fibroblasts, the resulting cell suspension was first incubated in mTEC-basic media (Supplementary Table 1) on Primaria plates (Corning-Costar, 353801) at 37 °C with 5% CO_2 for 4–5 h to allow preferential fibroblast attachment. Following incubation, non-adherent epithelial cells were collected by centrifugation (220 x *g*, 5 min), resuspended in mTEC-plus media (Supplementary Table 2), and seeded at 5×10^4 cells/cm^2 onto collagen (Sigma-Aldrich, C3867)-coated (50 μg/mL) PET transwell inserts (SPL Life Science, 37006) with a 0.4 μm pore membrane placed in 12-well plates (SPL Life Sciences, 30012). Cells were cultured under submerged conditions at 37 °C with 5% CO_2 until confluence, with media supplied to both apical and basal chambers. mTEC-plus media was refreshed every other day during this period. Upon reaching confluency, the apical media was removed to initiate air-liquid interface (ALI) conditions. Simultaneously, the basal media was replaced with mTEC-differentiation media (Supplementary Table 3) lacking fetal bovine serum (FBS) and ROCK inhibitor. mTEC-differentiation media was replaced every other day, while the apical surface was gently rinsed with PBS (pH 7.4; Welgene, LB 004–02) every 2–3 days to remove accumulated mucus. To assess the effect of **19b** on MCCs, it was added to the basal chamber at a final concentration of 5 μM at ALI days 0–4. DMSO was used as vehicle control at a final concentration of 0.1% (*v*/v). Media containing **19b** was renewed every other day before analysis.

4.9. mTECs immunofluorescence staining

For immunofluorescence staining, transwell cultures were rinsed twice with PBS to remove apical mucus. Cells were fixed with 4% paraformaldehyde (PFA) applied to both apical and basal chambers for 15 min at RT. After fixation, they were washed thrice with PBS and permeabilized in PBSTX (PBS containing 0.5% Triton X-100 (Sigma-Aldrich, 11332481001)) for 1 h on an orbital shaker (50–80 rpm). The apical compartment was then rinsed twice with PBS and blocked with 2% bovine serum albumin (BSA), 5% goat serum, and 0.2% Triton X-100 in PBS for 1 h at RT or O/N at 4 °C. Cells were incubated O/N at 4 °C in dark with antibodies diluted in blocking buffer (2% BSA, 5% goat serum, and 0.1% Triton X-100 in PBS): anti-acetylated α-tubulin conjugated

with Alexa Flour 488 (1:100; Cell signaling, 8058S) or anti-ZO-1 conjugated with Alexa Flour 594 (1:500; Invitrogen, 339194). The following day, they were washed thrice for 10 min with PBS. The transwell membranes were excised using forceps and a scalpel, placed cell-side up on glass slides, and mounted with Prolong Gold antifade reagent (Vector Laboratories, H-1900). Coverslips (Marienfeld, HSU-0101152) were placed on top of the transwell membranes and their edges were sealed with nail polish, dried for 10 min, and imaged with a confocal laser scanning microscope (LSM900, Zeiss). Images were analyzed using Fiji (ImageJ, NIH) with the Bio-Formats plugin [19].

4.10. qPCR

Total RNA was extracted from mTECs treated with DMSO or **19b** using TRI Reagent (Molecular Research Center, TR 118) according to the manufacturer's protocol. First-strand cDNA was synthesized using the TOPscript cDNA Synthesis Kit (Enzynomics, EZ005S). Real-time PCR was performed with *Foxj1*-specific primers (forward: 5′-GAG CTG GAA CCA CTC AAA GG-3′; reverse: 5′-GGT AGC AGG GCA GTT GAT GT-3′) using TOPreal qPCR 2× PreMIX (SYBR Green with low ROX; Enzynomics, RT500M) on a Rotor-Gene Q Real-Time PCR cycler (Corbett Research). The reaction was run in three technical replicates and *18S rRNA* (*Rn18s*; forward: 5′-GGG GAA TCA GGG TTC GAT-3′; reverse: 5'-GGC CTC GAA AGA GTC CTG TA-3′) was used for normalization. Relative gene expression (fold change) was calculated using the $\Delta\Delta C_t$ method [20]. in Microsoft Excel (Excel 2019) and the results were plotted using GraphPad Prism (version 9.3.0).

4.11. Statistical analysis

All statistical analyses were conducted using GraphPad Prism (version 9.3.0). Data are presented as mean ± standard deviation (SD), with error bars representing SD. Comparisons between two groups were evaluated using an unpaired Student's *t*-test. For comparisons involving three or more groups, one-way or two-way ANOVA was applied, followed by Tukey's honest significant difference (HSD) post hoc test. A P value <0.05 was considered statistically significant.

CRediT authorship contribution statement

Gwi Bin Lee: Writing – review & editing, Writing – original draft, Project administration, Investigation, Conceptualization. **Gopalakrishnan Chandrasekaran:** Data curation. **Da Bin Jeon:** Data curation. **Chan-Young Park:** Data curation. **Parvathi Varier Sundareswaran:** Data curation. **Byeong Wook Choi:** Resources. **Pyeongkeun Kim:** Resources. **Jihyeon Yoon:** Resources. **Seok-Yong Choi:** Writing – review & editing, Project administration, Methodology, Conceptualization. **Jin Hee Ahn:** Writing – review & editing, Project administration, Funding acquisition, Conceptualization.

Declaration of competing interest

The authors declare that they have no known competing financial interests or personal relationships that could have appeared to influence the work reported in this paper.

Acknowledgments

This work was supported by the National Research Foundation of Korea (NRF) grant funded by the Korea government (MSIT) (RS-2024-00348338, RS-2024-00411137) and Korea Drug Development Fund (RS-2021-DD116747).

Appendix A. Supplementary data

Supplementary data to this article can be found online at https://doi.org/10.1016/j.rechem.2026.103078.

Data availability

Data will be made available on request.

IV. Reference

[1] C. Ringers, E.W. Olstad, N. Jurisch-Yaksi, The role of motile cilia in the development and physiology of the nervous system, Philos. Trans. R. Soc. B 375 (1792) (2020) 20190156, https://doi.org/10.1098/rstb.2019.0156.
[2] R.M. Hyland, S.L. Brody, Impact of motile ciliopathies on human development and clinical consequences in the newborn, Cells 11 (1) (2022) 125, https://doi.org/10.3390/cells11010125.
[3] R.L. Huizar, C. Lee, A.A. Boulgakov, A. Horani, F. Tu, E.M. Marcotte, S.L. Brody, J. B. Wallingford, A liquid-like organelle at the root of motile ciliopathy, eLife 7 (2018) e38497, https://doi.org/10.7554/eLife.38497.
[4] J.A. Deane, S.D. Ricardo, Chapter six - Emerging Roles for Renal Primary Cilia in Epithelial Repair, in: K.W. Jeon (Ed.), International Review of Cell and Molecular Biology 293, Academic Press, 2012, pp. 169–193, https://doi.org/10.1016/B978-0-12-394304-0.00011-7.
[5] A. Grochowsky, M. Gunay-Aygun, Clinical characteristics of individual organ system disease in non-motile ciliopathies, Transl. Sci. Rare Dis. 4 (1–2) (2019) 1–23, https://doi.org/10.3233/TRD-190033.
[6] J. Wallmeier, D. Frank, A. Shoemark, T. Nöthe-Menchen, S. Cindric, H. Olbrich, N. T. Loges, I. Aprea, G.W. Dougherty, P. Pennekamp, et al., De novo mutations in FOXJ1 result in a motile ciliopathy with hydrocephalus and randomization of left/right body asymmetry, Am. J. Hum. Genet. 105 (5) (2019) 1030–1039, https://doi.org/10.1016/j.ajhg.2019.09.022.
[7] J. Zhang, G. Chandrasekaran, W. Li, D.-Y. Kim, I.Y. Jeong, S.-H. Lee, T. Liang, J. Y. Bae, I. Choi, H. Kang, et al., Wnt-PLC-IP3-Connexin-Ca2+ axis maintains ependymal motile cilia in zebrafish spinal cord, Nat. Commun. 11 (1) (2020) 1860, https://doi.org/10.1038/s41467-020-15248-2.
[8] I. Mukherjee, S. Roy, S. Chakrabarti, Identification of important effector proteins in the FOXJ1 transcriptional network associated with Ciliogenesis and ciliary function, Front. Genet. 10 (2019), https://doi.org/10.3389/fgene.2019.00023. Original Research.
[9] M. Wirschell, H. Olbrich, C. Werner, D. Tritschler, R. Bower, W.S. Sale, N.T. Loges, P. Pennekamp, S. Lindberg, U. Stenram, et al., The nexin-dynein regulatory complex subunit DRC1 is essential for motile cilia function in algae and humans, Nat. Genet. 45 (3) (2013) 262–268, https://doi.org/10.1038/ng.2533.
[10] X. Yu, C.P. Ng, H. Habacher, S. Roy, Foxj1 transcription factors are master regulators of the motile ciliogenic program, Nat. Genet. 40 (12) (2008) 1445–1453, https://doi.org/10.1038/ng.263.
[11] D.T. Grimes, C.W. Boswell, N.F. Morante, R.M. Henkelman, R.D. Burdine, B. Ciruna, Zebrafish models of idiopathic scoliosis link cerebrospinal fluid flow defects to spine curvature, Science 352 (6291) (2016) 1341–1344, https://doi.org/10.1126/science.aaf6419.
[12] J.L. Stubbs, I. Oishi, J.C. Izpisúa Belmonte, C. Kintner, The forkhead protein Foxj1 specifies node-like cilia in Xenopus and zebrafish embryos, Nat. Genet. 40 (12) (2008) 1454–1460, https://doi.org/10.1038/ng.267.
[13] G.B. Lee, G. Chandrasekaran, H.-J. Kim, P. Kim, J. Yoon, B.W. Choi, S.-H. Lee, S.-Y. Lee, D.-S. Shin, B.H. Lee, et al., Discovery of novel arylpyridine derivatives for motile ciliogenesis, Eur. J. Med. Chem. 277 (2024) 116764, https://doi.org/10.1016/j.ejmech.2024.116764.
[14] M. Lewis, T.H. Stracker, Transcriptional regulation of multiciliated cell differentiation, in: Seminars in cell & developmental biology 110, Elsevier, 2021, pp. 51–60, https://doi.org/10.1016/j.semcdb.2020.04.007.
[15] A. Caron, X. Xu, X. Lin, Wnt/β-catenin signaling directly regulates Foxj1 expression and ciliogenesis in zebrafish Kupffer's vesicle, Development 139 (3) (2012) 514–524, https://doi.org/10.1242/dev.071746.
[16] A. Tasca, M. Helmstädter, M.M. Brislinger, M. Haas, B. Mitchell, P. Walentek, Notch signaling induces either apoptosis or cell fate change in multiciliated cells during mucociliary tissue remodeling, Dev. Cell 56 (4) (2021) 525–539, e526, https://doi.org/10.1016/j.devcel.2020.12.005.
[17] C. Boutin, P. Labedan, J. Dimidschstein, F. Richard, H. Cremer, P. André, Y. Yang, M. Montcouquiol, A.M. Goffinet, F. Tissir, A dual role for planar cell polarity genes in ciliated cells, Proc. Natl. Acad. Sci. 111 (30) (2014) E3129–E3138, https://doi.org/10.1073/pnas.1404988111.
[18] Renato T. Skerlj, D. B., Gary J. Bridger., Facile Cyanomethylation of Bromopyridines by nucleophilic substitution with Lithioacetonitrile, Synlett 10 (2000) 1488–1490, https://doi.org/10.1055/s-2000-7644.
[19] M. Linkert, C.T. Rueden, C. Allan, J.M. Burel, W. Moore, A. Patterson, B. Loranger, J. Moore, C. Neves, D. Macdonald, et al., Metadata matters: access to image data in the real world, J. Cell Biol. 189 (5) (2010) 777–782, https://doi.org/10.1083/jcb.201004104.
[20] S.C. Taylor, K. Nadeau, M. Abbasi, C. Lachance, M. Nguyen, J. Fenrich, The ultimate qPCR experiment: producing publication quality, reproducible data the first time, Trends Biotechnol. 37 (7) (2019) 761–774, https://doi.org/10.1016/j.tibtech.2018.12.002.